Real Time Photon-Counting Receiver for High Photon Efficiency Optical Communications

Brian E. Vyhnalek
Advanced High Frequency Branch
NASA Glenn Research Center
Cleveland, OH, USA
brian.e.vyhnalek@nasa.gov

Jennifer M. Nappier, Sarah A. Tedder
Optics and Photonics Branch
NASA Glenn Research Center
Cleveland, OH, USA

***Abstract*—We present a scalable design for a photon-counting ground receiver based on superconducting nanowire single photon detectors (SNSPDs) and field programmable gate array (FPGA) real-time processing for applications to space-to-ground photon starved links, such as the Orion EM-2 Optical Communication Demonstration (O2O) [1], and future deep space or low transmitter power missions. The receiver is designed to receive a serially concatenated pulse position modulation (SCPPM) waveform [2], which follows the Consultative Committee for Space Data Systems (CCSDS) Optical Communications Coding and Synchronization Red Book standard [3]. The receiver design uses multiple individually fiber coupled, 80% detection efficiency commercial SNSPDs in parallel to scale to a required data rate, and is capable of achieving data rates up to 528 Mbps. For efficient fiber coupling from the telescope to the array of parallel detectors that can be scaled both to telescope aperture size and the number of detectors, we use either a single mode fiber (SMF) photonic lantern or a few-mode fiber (FMF) photonic lantern [4]. In this paper we give an overview of the receiver system design, the characteristics of the photonic lanterns, the performance of the SNSPDs, and system level tests. We show that 40 Mbps can be received using a single SNSPD, and discuss aspects for scaling to higher data rates.**

***Index Terms*—optical communications, single photon detectors, superconducting nanowire, few-mode fibers**

I. Introduction

With demonstrations such as NASA's Lunar Laser Communications Demonstration (LLCD) showing that high-rate free-space optical communications links from cis-Lunar space are not only achievable, but comparable or exceed the fastest Ka-band RF links [5], space-to-Earth optical communications is increasingly a viable communications system option. Furthermore NASA has several upcoming optical communications demonstrations: the Laser Communication Relay Demonstration (LCRD) [6] providing all-optical high-rate communications from geostationary orbit, the Orion EM-2 Optical communications demonstration (O2O) [1], an 80 - 250 Mbps direct-to-Earth link capability for the crewed mission aboard the Orion Multi-Purpose Crew Vehicle (OMPCV) from lunar distances, and the Deep Space Optical Communication (DSOC) Project [7], a demonstration of laser communications flight transceiver and ground receiver technology from 0.1-2 astronomical units (AU), to be hosted aboard the Psyche Mission spacecraft [8]. The success of these upcoming missions will continue motivate the adoption of optical communications for mission-operational infusion.

While the upcoming optical communication demonstrations will continue to validate capabilities, considerations are also being given to cost-effective ground terminal technologies that are both scalable and assembled from commercial-off-the-shelf (COTS) components. Ideally a system could be designed that could support a variety of data rates, telescope aperture sizes, and environmental factors such as background light and atmospheric turbulence levels. In this paper we discuss a concept for a scalable design, and the development of a real-time photon counting optical communications receiver system including the aft optics, single photon detectors, and a real-time field programmable gate array (FPGA) based digital receiver.

II. Receiver Overview

In a direct-detection photon-counting optical communication system the basic receiver architecture consists of a telescope aperture for light collection and focusing, and a photosensitive surface that converts the detected optical intensity into an electrical signal. For the highest sensitivity, superconducting nanowire single photon detectors (SNSPDs) may be used, but must operate at cryogenic temperatures. Options for coupling to cryogenic SNSPDs are either through fiber-optic, or free-space coupling, but both can present challenges for efficiency and scalability.

A. Photonic Lantern

The atmosphere causes distortions to the spatial profile of the transmitted beam, sending energy into higher-order spatial modes. To mitigate this effect some options include coupling through single-mode fiber (SMF), multi-mode fiber (MMF), or free-space coupling to larger area SNSPDs and/or multi-element SNSPD arrays [9], [10]. Fiber coupling offers a more flexible receiver design, however without adaptive optics significant losses are incurred when coupling to SMF, and coupling current commercial SNSPDs to MMF is inefficient and complex, requiring cryogenic focusing optics since these devices are designed for SMF. Larger area SNSPDs are in development, but offer lower count rates, higher dark counts, higher jitter, and lower yield. Interleaved SNSPD on-chip

arrays can cover larger areas, but this technology is mainly in research development and only beginning to emerge commercially.

Another possible solution for fiber coupling is the photonic lantern (Figure 1a, 1b), which has been used for astronomical applications for several years [11]. The photonic lantern is a low-loss fiber optic device that connects one multi-mode core to several smaller cores that propagate less modes. Often the smaller cores are SMF, but they can also be larger core few-mode fiber (FMF) [4]. Such a device is fabricated by inserting

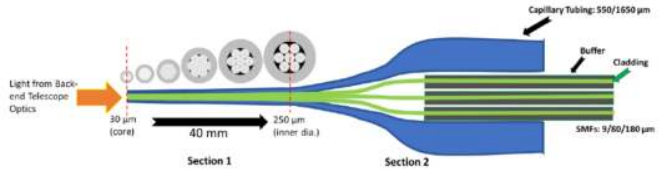

(a)

(b)

Fig. 1: (a) Photonic lantern diagram. (b) Prototype photonic lantern designed and fabricated at NASA GRC.

N SMFs (or FMFs) into a cylindrical glass capillary, and then is heated and drawn to form an adiabatic taper transition to a MMF input port. For maximum throughput, the total number of guided modes in the output legs must sum to the number of guided modes in the MMF port, approximately given by

$$N \approx \left(\frac{\pi d \mathrm{NA}}{2\lambda} \right)^2 , \qquad (1)$$

where d is the MMF core diameter, NA is the MMF numerical aperture, and λ is the operating wavelength. Thus, to detect all the light collected by the lantern, each output fiber must be coupled to an individual detector. As atmospheric turbulence increases and the energy is scattered into higher order spatial modes, the number of detectors needed increases accordingly. Depending on the condition and desired data rate, the number of detectors needed could be higher than the number of detectors required to compensate for detector dead time. Since a typical MMF can support 10s to 100s of modes, the number of detectors in parallel would become prohibitively large. Hence our solution that we are considering is MMF to FMF photonic lanterns, in which the the output FMFs are designed to couple as efficiently as SMF to commercial SNSPDs.

B. Single-Photon Detectors

A key enabling technology for advanced light detection at IR wavelengths are supercoducting nanowire single-photon detectors (SNSPDs). SNSPDs have been demonstrated to offer superior performance in detection effciency, timing resolution, and count rates over semiconductor InGaAs photodetectors and photomultiplier tubes (PMTs) [12]. For optical communications applications SNSPDs, specifically SNSPD arrays, have already been demonstrated in a space-to-ground link as an integral component for the LLCD receiver [5], [9], and additionally will be used for the upcoming DSOC demonstration [7]. However, only recently have SNSPDs become commercially available. With several commercial vendors offering turnkey multichannel SNSPD systems with simplified cryogenics, SNSPDs are increasingly viable as an operational component for space-to-ground high-photon efficiency free-space optical communications links. We have characterized

(a)

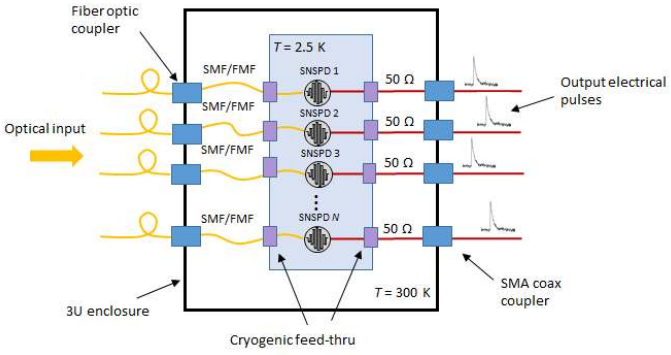

(b)

Fig. 2: (a) Opus One™ SNSPD system. (b) Functional diagram.

a commercial two-channel, SMF-coupled, and two-channel FMF-coupled SNSPD system from Quantum Opus, LLC (Figure 2a). The base system consists of a two-stage closed-cycle helium cryocooler with a 2.5 K second stage on which the

SNSPDs are mounted, enclosed in a 3U rack-mountabe box. Efficient coupling from the detectors to single-mode or 20 μm, graded-index few-mode optical fiber is achieved through fiber self-alignment [13], [14], and the fibers are routed through cryogenic feed-thrus to the inputs on the front of the enclosure (Figure 2b). Electrically the devices are current biased with adjustable front panel controls, and coupled to 50 Ω coaxial readout cables to room temperature amplifiers with 500 MHz bandwidth and a maximum 55.6 dB gain [15]. This system is powered via a Standford Research Systems SIM900 mainframe, and can be computer controlled either serially or through GPIB interface.

In our characterization we have assessed detection efficiency for SMF and FMF-coupled detectors at an operating wavelength of 1550 nm (Figure 3), in addition to count rate (Figure 4), and timing jitter (Figure 5) [16], [17]. As shown in

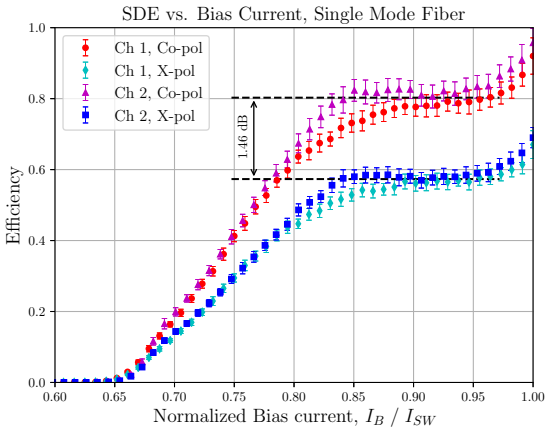

Fig. 3: System detection efficiency dependence on bias current for SMF. The optical input to the fibers was single-mode, thus the FMF-coupled detector efficiency is essentially identical.

Figure 3, the system detection efficiency reaches an average maximum value of $\approx$ 80%. The SNSPDs have a polarization dependency, thus we also show the worst case (x-pol) detection efficiency, which is $\approx$ 1.5 dB worse.

In Figure 4 we show output counts under variable levels of input intensity with the detectors at a fixed bias for maximum efficiency, and ideal polarization. The output counts follow a log-linear response before tending to apparent saturation at an output count rate of $\approx$ 60 Mcps. An absolute maximum count rate, approaching $\approx$ 80 - 100 Mcps was measured as relaxation oscillation set in at input flux rates on the order of 10s of G-ph/s.

The detection jitter, shown in Figure 5, was determined by measuring the input response function (IRF) of the detectors when illuminated with femtosecond laser pulses, in which each pulse was attenuated to $\ll$ 1 photon per pulse. The jitter was then calculated from the FWHM of the IRF. From the graph, the jitter decreases with increasing bias current, approaching values $\approx$ 50 - 80 ps. For PPM-based optical

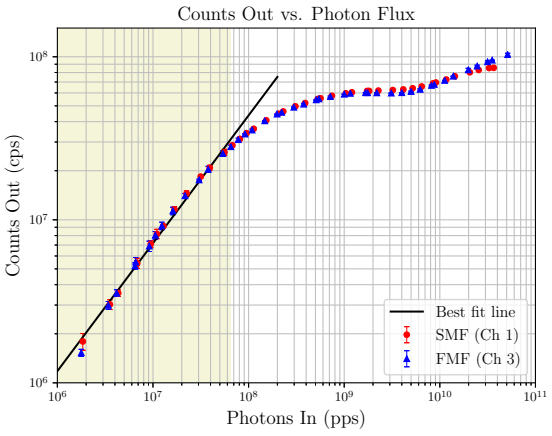

Fig. 4: Output count rate dependence on input photon flux. The highlighted area is the approximate (log) linear response region where the detection efficiency is reduced by 3 dB.

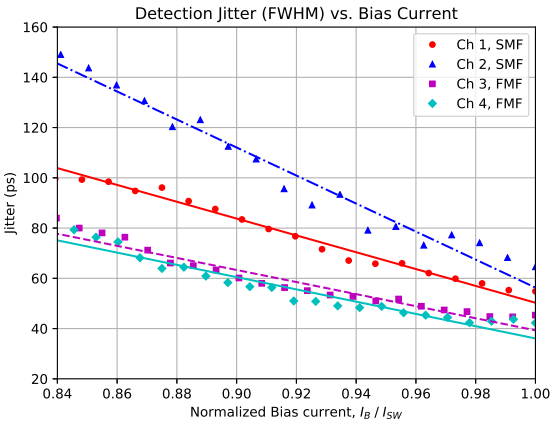

Fig. 5: Detection jitter dependence on bias current.

communications, ideally the jitter should be as small a fraction of the transmission slot period as possible. Practically, less than 20% is recommended. Hence for 500 ps slot rates, the jitter should be less than 100 ps, which is easily achieved.

III. System Testing

An optical test bed was designed to emulate the transmitter and receiver of photon counting optical communications links [18]. A block diagram of the system is shown in Figure 6, and a description of the optical transmitter, link emulation, and optical receiver follows.

A. Optical Transmitter

The optical transmitter consists of a software defined radio (SDR), and a pair of high-extinction ratio electro-optic (EO) modulators cascaded in series which modulates a continuous wave laser with the electrical pulse output from the SDR. The EO modulators are cascaded in series and driven differentially

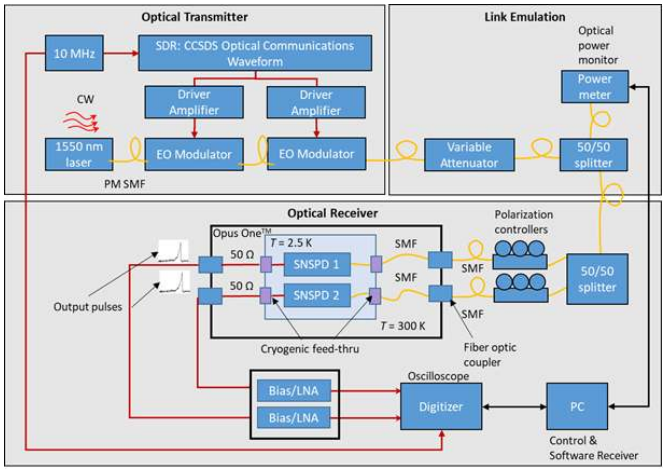

Fig. 6: Optical communications link testbed.

using the positive and negative low voltage differential signaling (LVDS) components of the FPGA to achieve pulse narrowing and extinction ratios $\geq\approx$ 40 dB for PPM modulation orders M = 16 and higher [19].

The SDR consists of a Harris Corporation Reconfigurable Space Processor (RSP) development card, and a custom optical mezzanine card developed at NASA Glenn Research Center [20]. The RSP contains two Xilinx Virtex 7 FPGAs, a digital signal processor (DSP), and supplemental memory, and is controlled with a computer through the SpaceWire interface. Serialization of the waveform signal, which is sent out in parallel from the FPGA, is performed by the optical mezzanine card. The optical mezzanine card can generate a 2 GHz slot clock or can accept a slot clock from an external source. It divides the slot clock by 16 and sends it to the FPGA. The FPGA sends 16 parallel data lines to the optical mezzanine card, which then converts them into a serial stream. This serial data interfaces to the EO modulator setup.

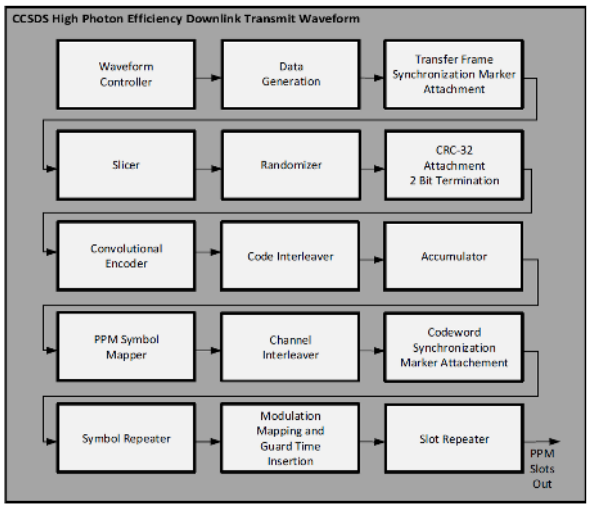

Fig. 7: Transmit waveform block diagram.

The optical waveform is targeted to one of the Xilinx Virtex 7 FPGAs on the Harris RSP, and implements the CCSDS Optical Communications Coding and Synchronization Red Book High Photon Efficiency telemetry link (Figure 7) [3]. This includes modulation orders M = 4, 8, 16, 32, 64, 128, and 256; and code rates 1/3, 1/2, and 2/3. Pseudorandom bit stream (PRBS) data is generated on the platform as a part of this waveform. The channel interleaver is implemented in the waveform, but has been bypassed for system testing. The waveform combined with the optical mezzanine card can generate PPM slot widths from 0.5 ns to 512 ns.

B. Link Emulation

The photon counting optical communications link free space loss is emulated with a fiber digital variable attenuator, used to change the signal power going into the receiver. A 50/50 fiber splitter is used to provide a test port for measuring optical power with a power meter, which is controlled by a computer. No external noise is inserted. The only noise in the system is blackbody induced dark counts on the order of a few hundred counts per second, since there is no filtering in the current set up. With appropriate filtering, the dark counts with SMF-coupled detectors is a few 10s of Hz [16].

C. Optical Receiver

The photon counting optical receiver for this test setup consists of a 50/50 fiber splitter, fiber polarization controllers for each detector channel, two SNSPDs, detector bias and amplification, a digitizer, and a software model of the optical receive waveform. The attenuated signal from the optical transmitter is split so that the two detectors can receive the transmitted signal simultaneously. The polarization controllers are used to maximize the photon counts out of the detectors by optimizing the polarization alignment.

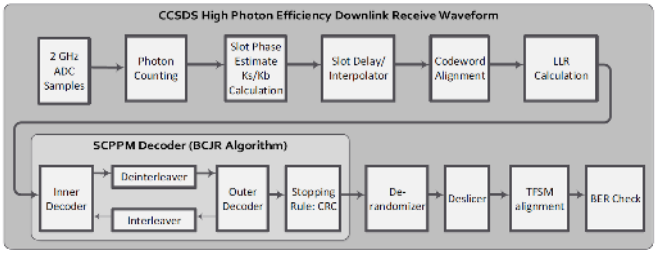

Fig. 8: Receiver waveform block diagram.

An oscilloscope is used to digitize and save the pulses output from the SNSPDs. A computer is used to sample the detector pulses simultaneously with the power meter readings in order to verify the input power into the detectors is constant throughout the data capture. The clocks of the transmitter SDR and the receiver digitizer are locked for this test in order to eliminate error caused by clock recovery. The pulses are digitized at a rate of 2 GSps and post-processed using a MATLAB receiver (Figure 8). The MATLAB receiver performs slot and symbol recovery. Once the slot and symbol

boundaries have been calculated, the receiver slot recovery algorithm delays and interpolates the incoming detector pulse samples. A threshold is used to find the rising edge of the interpolated pulses and this data is down-sampled to count photon counts per slot. The rise time of the detector pulses is 850 ps and the pulses are sampled at a rate of 2 GHz. Since the sample rate does not meet the required Nyquist frequency, additional jitter of approximately 45 ps is introduced. The total jitter is 61 ps RMS for channel 1 and 68 ps RMS for channel 2. As a part of the slot and symbol recovery algorithm, the signal photon counts per signal slot (Ks) and the background photon counts per slot (Kb) are also calculated. Once the symbol and slot boundaries are calculated, the receiver then performs code word alignment and calculates the log likehood ratios (LLRs) for each slot. SCPPM iterative decoding is completed using the Bahl, Cocke, Jelinek and Raviv (BCJR) algorithm. The decoded data is then de-randomized and de-sliced before the transfer frames are synchronized and a bit error rate on the PRBS data is calculated.

IV. Testing Results

System testing was conducted using the optical transmitter and receiver system test setup described in Section III. The waveform selected was the PPM-32, code rate 1/3, slot width 1 ns, 40 Mbps waveform. This waveform was selected because it is the lowest PPM order and smallest slot width that a single detector could successfully receive error free. The detector blocking time of 20 ns was found to have a low impact on the performance of this waveform. Bit error rate (BER) curve results from the system testing are presented Figure 9.

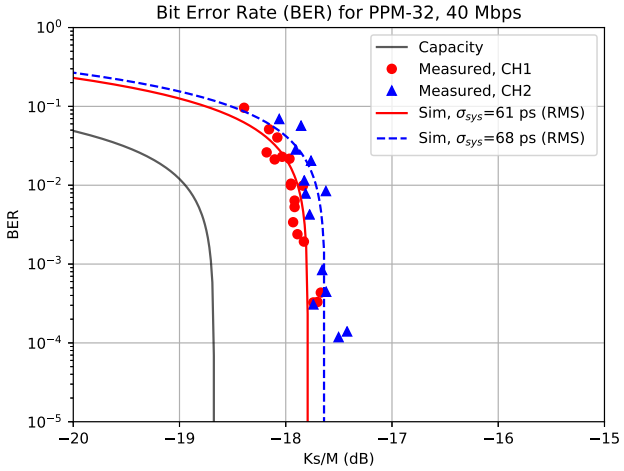

Fig. 9: Optical link testing BER curve results for PPM-32, 40 Mbps waveform with $K_b \approx 0.0001$. The simulation curves are for two different total system jitter, and an assumed 20 ns detector dead time.

Also shown are results from 60 ps and 68 ps RMS jitter simulations. As can be seen in the graph, detector channel 1 (red circles) is slightly to the left of detector channel 2 (blue triangles). From Figure 5 channel 1 has less jitter than channel 2, and so it performs slightly better. The system predicted jitter values of 61 and 68 ps RMS match very closely to the simulation results and the system test results.

V. System Scaling

For a given rate, modulation, required detected signal level Ks/M, BER, and desired margin, there is a trade between required number of detectors and total received signal photons per pulse. By combining the outputs from multiple photon detectors in parallel, the system architecture can be scaled to meet specific data rates and power requirements. Figures 10a and 10b show two examples of simulated photon counts per signal slot vs. number of detector channels. The dark horizontal lines show the Ks/M levels for capacity and the

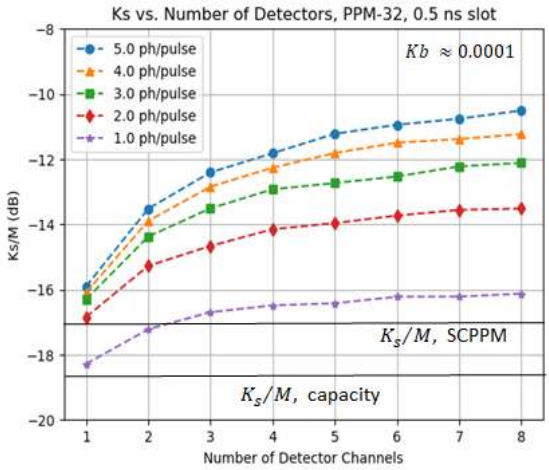

(a)

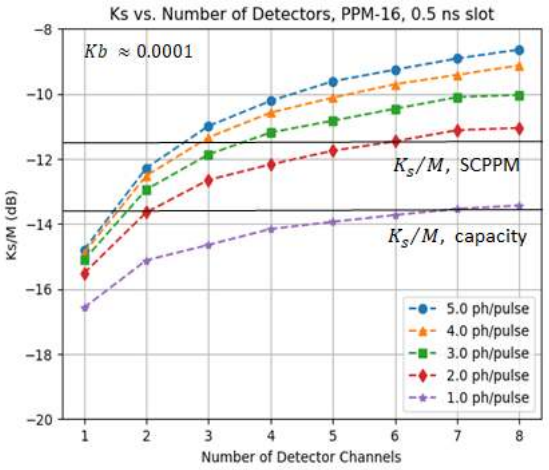

(b)

Fig. 10: Photon counts per signal slot vs. number of detectors for (a) PPM-32, and (b) PPM-16.

performance of SCPPM, respectively. Based on the required Ks/M level and desired link margin, we can determine the number of parallel detectors and number of received photons per pulse required.

VI. Conclusion and Future Work

We characterized a commercial superconductor nanowire single-photon detector system with improved detector count rates, and explored coupling to few-mode fibers (FMF). Parameters such as detection efficiency, dark count rate, reset time, maximum count rate, and timing jitter were assessed. With a single detector a 40 Mbps communications link was closed error-free, and the BER results validated our simulation model. Future work will include communication link performance improvement through combining multiple detector channels to achieve higher rates, multi-mode to single-mode and multi-mode to few-mode fiber photonic lantern characterization, and link performance with emulated atmospheric turbulence. Finally we will to implement the MATLAB receiver model onto FPGA to complete the real-time receiver implementation.

References

[1] B. S. Robinson, T. Shih, F. I. Khatri, D. M. Boroson, J. W. Burnside, O. Guldner, S. Constantine, J. Torres, T. M. Yarnall, C. E. DeVoe, W. Hubbard, D. J. Geisler, M. L. Stevens, O. Mikulina, N. W. Spellmeyer, J. P. Wang, R. Butler, M. Hogan, T. King, and A. Seas, "Laser communications for human space exploration in cislunar space: ILLUMA-T and O2O," in *Free-Space Laser Communication and Atmospheric Propagation XXX*, H. Hemmati and D. M. Boroson, Eds., vol. 10524, International Society for Optics and Photonics. SPIE, 2018, pp. 231 – 235.

[2] B. Moison and J. Hamkins, "Coded modulation for the deep-space optical channel: Serially concatenated pulse position modulation," *The Interplanetary Network Progress Report*, vol. 42, no. 161, 2005.

[3] *Optical Communications Coding and Synchronization Draft Recommended Standard, 142.0-R-1 Red Book*, Consultative Committee for Space Data Systems (CCSDS), 2018.

[4] S. A. Tedder, B. E. Vyhnalek, S. Leon-Saval, C. Betters, B. Floyd, J. Staffa, and R. Lafon, "Single-mode fiber and few-mode fiber photonic lanterns performance evaluated for use in a scalable real-time photon counting ground receiver," in *Free-Space Laser Communications XXXI*, H. Hemmati and D. M. Boroson, Eds., vol. 10910, International Society for Optics and Photonics. SPIE, 2019, pp. 69 – 78.

[5] B. S. Robinson, D. M. Boroson, D. A. Burianek, D. V. Murphy, F. I. Khatri, J. W. Burnside, J. E. Kansky, A. Biswas, Z. Sodnik, and D. M. Cornwell, "The NASA lunar laser communication demonstration - successful high-rate laser communications to and from the moon," in *AIAA - SpaceOps 2014*, 2014.

[6] E. Luzhanskiy, B. Edwards, D. Israel, D. Cornwell, J. Staren, N. Cummings, T. Roberts, and R. Patschke, "Overview and status of the laser communication relay demonstration," in *Free-Space Laser Communication and Atmospheric Propagation XXVIII*, H. Hemmati and D. M. Boroson, Eds., vol. 9739, International Society for Optics and Photonics. SPIE, 2016, pp. 100 – 113.

[7] A. Biswas, M. Srinivasan, S. Piazzolla, and D. Hoppe, "Deep space optical communications," in *Free-Space Laser Communication and Atmospheric Propagation XXX*, H. Hemmati and D. M. Boroson, Eds., vol. 10524, International Society for Optics and Photonics. SPIE, 2018, pp. 242 – 252.

[8] D. Y. Oh, S. Collins, D. Goebel, B. Hart, G. Lantoine, S. Snyder, G. Whiffen, L. Elkins-Tanton, P. Lord, Z. Pirkl, and L. Rotlisburger, "Development of the Psyche Mission for NASA's Discovery Program," in *35th International Electric Propulsion Conference*. Georgia Institute of Technology, October 2017.

[9] M. E. Grein, A. J. Kerman, E. A. Dauler, O. Shatrovoy, R. J. Molnar, D. Rosenberg, J. Yoon, C. E. DeVoe, D. V. Murphy, B. S. Robinson, and D. M. Boroson, "Design of a ground-based optical receiver for the lunar laser communications demonstration," in *2011 International Conference on Space Optical Systems and Applications (ICSOS)*, 2011.

[10] M. D. Shaw, F. Marsili, A. D. Beyer, J. A. Stern, G. V. Resta, P. Ravindran, S. Chang, J. Bardin, D. S. Russell, J. W. Gin, F. D. Patawaran, V. B. Verma, R. P. Mirin, S. W. Nam, and W. H. Farr, "Arrays of WSi superconducting nanowire single photon detectors for deep-space optical communications," in *CLEO: 2015*. OSA Technical Digest (online) (Optical Society of America, 2015), paper JTh2A.68.

[11] T. A. Birks, I. Gris-Sánchez, S. Yerolatsitis, S. G. Leon-Saval, and R. R. Thomson, "The photonic lantern," *Adv. Opt. Photon.*, vol. 7, no. 2, pp. 107–167, Jun 2015.

[12] C. M. Natarajan, M. G. Tanner, and R. H. Hadfield, "Superconducting nanowire single-photon detectors physics and applications," *Superconductor Science and Technology*, vol. 25, no. 6, 2012.

[13] *Nanowire Datasheet*, Quantum Opus, Jan 2017.

[14] A. J. Miller, A. E. Lita, B. Calkins, I. Vayshenker, S. M. Gruber, and S. W. Nam, "Compact cryogenic self-aligning fiber-to-detector coupling with losses below one percent," *Optics Express*, vol. 19, no. 10, pp. 9102 – 9110, May 2011.

[15] *Nanowire Bias and Readout Electronics Datasheet*, Quantum Opus, Jan 2017.

[16] B. E. Vyhnalek, S. A. Tedder, and J. M. Nappier, "Performance and characterization of a modular superconducting nanowire single photon detector system for space-to-Earth optical communications links," in *Free-Space Laser Communication and Atmospheric Propagation XXX*, H. Hemmati and D. M. Boroson, Eds., vol. 10524, International Society for Optics and Photonics. SPIE, 2018, pp. 369 – 377.

[17] B. E. Vyhnalek, S. A. Tedder, E. J. Katz, and J. M. Nappier, "Few-mode fiber coupled superconducting nanowire single-photon detectors for photon efficient optical communications," in *Free-Space Laser Communications XXXI*, H. Hemmati and D. M. Boroson, Eds., vol. 10910, International Society for Optics and Photonics. SPIE, 2019, pp. 62 – 75.

[18] J. M. Nappier, B. E. Vyhnalek, S. A. Tedder, and N. C. Lantz, "Characterization of a photon counting test bed for space to ground optical pulse position modulation communications links," in *Free-Space Laser Communications XXXI*, H. Hemmati and D. M. Boroson, Eds., vol. 10910, International Society for Optics and Photonics. SPIE, 2019, pp. 53 – 60.

[19] N. C. Lantz, J. M. Nappier, B. E. Vyhnalek, and S. A. Tedder, "Optical software defined radio transmitter extinction ratio enhancement with differential pulse carving," in *Free-Space Laser Communications XXXI*, H. Hemmati and D. M. Boroson, Eds., vol. 10910, International Society for Optics and Photonics. SPIE, 2019, pp. 386 – 394.

[20] J. M. Nappier and N. C. Lantz, "Development of an optical slice for an RF and optical software defined radio," in *Free-Space Laser Communication and Atmospheric Propagation XXX*, H. Hemmati and D. M. Boroson, Eds., vol. 10524, International Society for Optics and Photonics. SPIE, 2018, pp. 384 – 394.